Chin. Geogra. Sci. 2011 21(5) 554–562
doi: 10.1007/s11769-011-0466-0
www.springerlink.com/content/1002-0063

Effective Solution Algorithm for Tomographic Inversion of Volume Emission Rate from Satellite-based Limb Measurement

WANG Zijun, CHEN Shengbo
(*College of Geoexploration Science & Technology, Jilin University, Changchun 130026, China*)

Abstract: The volume emission rate (VER) of airglow can be used to investigate atmospheric processes. Satellite-based limb measurement of atmosphere is able to obtain the VER profile of airglow with high vertical resolution. However, the traditional one-dimensional retrieval techniques for VER inversion fail to retrieve horizontal structure of VER profile. Thus, the tomographic technique based on the maximum probability is applied to retrieving two-dimensional VER profile of airglow from infrared limb measurement. This technique could process the observed data with low signal-to-noise ratio caused by the observation angle of less than 180° due to the solid nature of the Earth. For saving the processing time and improving the computing speed of VER inversion, serial tables for storing the large sparse matrix for radiance simulation and a large dataset during iterative estimate of VER are presented. The index and weighting factor of line of sight (LOS) through each grid are saved in initial estimate to avoid being computed repeatedly. Furthermore, the product of observed radiance and corresponding weighting factor obtained in initial iteration is stored as weighted observed radiance for the iterative calculation subsequently. Based on the improved algorithm, the VER of airglow is inversed through the tomographic technique. The full width of half maximum (FWHM) of error is 1.78% and the offset of the peak percentage error is 0.22% after 40 iterations for final VER. Comparison of assumed and retrieved VER profiles suggests that VER can be retrieved with a bias of 15% between 10 km and 90 km above the LayerMin (6384 km from the Earth center), and with a bias of 8% for altitude from 30 km to 60 km with vertical resolution of 1 km after 40 iterations. After improvements, the computation speed of VER inversion for once can be improved by 29.6 times for 700 images of 1/3 orbit, and accordingly, the processing time will be reduced from 3 hours and 11 minutes to only 6 minutes. In conclusion, the improvements to tomographic inversion of VER of airglow proposed in this paper are effective and significant.
Keywords: volume emission rate; tomographic technique; limb measurement; radiance; airglow

Citation: Wang Zijun, Chen Shengbo, 2011. Effective solution algorithm for tomographic inversion of volume emission rate from satellite-based limb measurement. *Chinese Geographical Science*, 21(5): 554–562. doi: 10.1007/s11769-011-0466-0.

1 Introduction

The airglow is considered to be the atomic and molecular emissions in the atmosphere, and the volume emission rate (VER) of airglow can be used for determining the trace gas density profile in the upper atmosphere (Khabibrakhmanov *et al*., 2002), obtaining the internal structure information of aurora form *etc*. (Evans and Llewellyn, 1972), and studying gravity waves (Frey *et al*., 2001). The molecular oxygen in the excited $O_2(a^1\Delta_g)$ state is formed directly by ozone photolysis in the Hartley band then radiates in the ozone infrared atmospheric (OIRA) band at 1.27μm (Wiensz, 2005). The VER of airglow in OIRA band have been used for determination of the density profile of ozone in the upper atmosphere by dispersed ground-based and rocket-balloon experiments (Evans and Llewellyn, 1972; McDade *et al*., 1991) as well as scientific satellites, e.g. the Swedish-led Odin satellite (Degenstein *et al*., 2003) and Solar Mesosphere Explorer (SME) (Rusch *et al*., 1984). Satellites can make

Received date: 2010-08-20; accepted date: 2010-12-06
Foundation item: Under the auspices of National High Technology Research and Development Program of China (No. 2006AA12Z102), Graduate Innovation Fund of Jilin University (No. 20091023)
Corresponding author: CHEN Shengbo. E-mail: chensb@jlu.edu.cn

atmosphere measurements globally compared to the ground-based observatory network (Degenstein, 1999). Traditional remote sensing method for one-dimensional (1D) information is based on the assumption that the upper atmosphere is homogenous at different altitudes. However, because the atmospheric constituent profiles depend on the solar input which varies necessarily with latitude. Thus, it is extremely important that two or even three dimensional structure information of the atmospheric constituent profiles with high spatial and temporal resolutions is known globally. Compared with the traditional nadir remote sensing, the remote sensing based on limb mode can make the integrated measurements of atmospheric emission rate along multiple lines of sight (LOSs) at different tangent heights, and improve the vertical resolution of retrieved VER profiles greatly and global coverage compared with the occultation mode (Noël *et al*., 2002; Degenstein *et al*., 2008).

One of the instruments applying this new limb remote sensing technique for probing the VER profile of airglow is the Optical Spectrograph and Infrared Imager System (OSIRIS) equipped on the satellite Odin, launched on February 21, 2001. OSIRIS is capable of observing infrared radiance in the band of 1.27 μm for determining the VER profiles (Solomon *et al*., 1984; Khabibrakhmanov *et al*., 2002). For this new atmospheric remote sensing technique, it is necessary to apply an algorithm to retrieve two-dimensional (2D) information from the line of sight observation (McDade and Llewellyn, 1993).

Tomographic techniques for reconstruction of 2D structure information have been applied to many fields, such as astronomy, microscopy, image processing and seism (Xu, 2003), and the application in the modern medical science is the most common. The emission tomography, applied in atmospheric infrared remote sensing, is similar to the transmission tomography applied in the medical science. The emitting atmosphere is analogous to a radioactive organ and the infrared instrument is similar to a rotating detector. The purpose of the emission tomography is to retrieve vertical cross sections of the atmospheric density distribution with higher resolution compared to the conventional remote sensing techniques (Fleming, 1982). The tomography could be summarized into two main categories, 2D algebraic reconstruction and filtered transform methods. 2D algebraic reconstruction techniques have been applied to Algebraic Reconstruction Technique (ART) (Gordonb *et al*., 1970), Multiplicative Algebraic Reconstruction Technique (MART) (Degenstein *et al*., 2003; Thomson and Tyler, 2007), and Maximum Likelihood Expectation Maximization Technique (MLEM) (Shepp and Vardi, 1982). Filtered transform techniques have been used in Radon transform (Cormack, 1963; Solomon *et al*., 1988), Abel transform (Roble and Hays, 1972; Dribinski *et al*., 2002), and Cormack transform (Cormack, 1964; Puro, 2001).

It is impossible for the linear integrals in a discrete fashion for airglow limb observations to cover 180° due to the solid nature of the Earth, which is required for an accurate tomographic inversion (Degenstein, 1999). Thus, this system of linear equations is sparse and overdetermined so that it can not be readily solved using standard direct matrix inversion methods. A solution algorithm based on maximum probability which is particularly robust and well suited for dealing with observations with relatively low signal-to-noise ratio made in a photon-counting mode is applied in this paper. Tomographic inversion requires the solution of a system of equations that consists of many linear integrals in a discrete fashion. Moreover, the inversion involves a large number of datasets and it will cost long time due to the complicated calculating process. This paper focused on the effective solution algorithm of tomographic inversion of VER, i.e. how to store the large sparse matrix and improve the computation speed.

2 Data and Methods

2.1 Data

The radiance measurements used for the retrieval of VER profile in this study are simulated using assumed VER profile. The ancillary parameters listed in Table 1

Table 1 Parameters of OSIRIS and satellite Odin

Item	Value
R_{sat} (orbit radius of satellite)	6978 km
Altitude of satellite	600 km
Inclination	97°
Vertical resolution for line of sight	1 km
Number of pixels	128
Field of view	2.03°
Tangent height of principal optical axis	40.5 km corresponding to 20 pixels
Satellite linear velocity	7.559 km/s
Satellite angular velocity	1.09×10^{-3} radian/s
Exposure frequency	0.5 Hz

for simulation are based on the OSIRIS equipped on the satellite Odin, which consists of a UV-visible optical spectrograph and an infrared imaging system for observing the limb emission of molecular oxygen.

2.2 Limb measurement simulation

2.2.1 Model of limb observation

Figure 1 is a typical limb geometry, the VER profile is assumed to exist throughout the atmospheric grid. The grid is bounded by the angle along the satellite orbit and the radial distance from the centre of the Earth. The grid index (j) increases with atmospheric layer and then with angular division. The first angular division is at an arbitrary ascending node. Three coordinate systems are defined, the ascending node (asc), the satellite (sat), and the instrument (inst) system, used for the simulation of infrared radiance. The ascending node coordination system is a fixed Earth centered three-dimensional Cartesian space, which is used to define the 2D VER profile. X-axis (X_{asc}) points towards the ascending node, the Z-axis (Z_{asc}) is rotated 90° from the X-axis along the satellite motion within the orbit plane and Y-axis is the direction which is perpendicular with the orbit plane. P_{asc} is the direction vector of a LOS, and S_{asc} is the position of satellite.

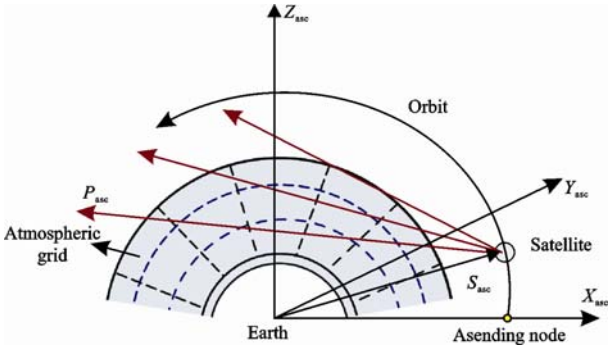

Fig. 1 Limb geometry in ascending node coordinate system

The infrared radiance transmitted through the atmospheric grid in the limb geometry illustrated in Fig. 1 along the LOSs with different tangent heights could be observed by instruments equipped on the satellite. The radiance (B) in any viewing direction could be defined by the integral of the VER ($E(s)$) along the LOS (s). If the satellite is used as the origin of viewing direction, the integral along a path from the satellite (sat) to infinity could be expressed as follows:

$$B = \int_{\text{sat}}^{\infty} E(s)\mathrm{d}s \tag{1}$$

For a single LOS i, the radiance (B_i) could be calculated by Equation (2).

$$B_i = \sum_j E_j L_{ij} \tag{2}$$

where E_j is the VER of grid j, and L_{ij} is the intercept of the ith LOS intersected with grid j.

2.2.2 Intercept determination

From Equation (2), the intercept is a necessary parameter which must be determined firstly. When the motion and orientation parameters of instrument equipped on the satellite and the relationship of transformations between three coordinate systems mentioned above are known, the direction vector (P_{asc}) of LOS can be calculated through the Equation (3).

$$\frac{x - S_x}{P_x} = \frac{y}{P_y} = \frac{z - S_z}{P_z} \tag{3}$$

where S_x and S_z are the x and z components of S_{asc} in the ascending node coordinate system; P_x, P_y and P_z are the x, y, z components of the direction vector P_{asc} respectively. The spherical equation family of atmospheric grids and the linear equation family of angular division could be given as equations (4) and (5) respectively.

$$x^2 + y^2 + z^2 = r^2 \tag{4}$$

$$z = x \tan\gamma \tag{5}$$

where r is the radial distance; γ is the angular division along the orbit direction.

The line of sight intersects with the atmospheric layer and angular division of grid. The coordinates of all the intersecting nodes along the LOS are calculated respectively by the equations (3) to (5). They are collocated and saved according to their coordinates x in an ascending order. Thus, the intercept of LOS through each grid can be determined by the coordinates of the adjacent two points. The index of each grid that intercepted by LOS is also calculated by angular and atmospheric layer index for the later simulation.

2.3 Tomographic inversion

2.3.1 Tomography

The key principle of tomography is Radon transformation which is established by Radon (Xu, 2003). The clas-

sic Radon transformation is defined as the integral of function $f(x, y)$ along the line (L) shown as Equation (6).

$$p = \int_{\mathrm{L}} f(x, y)\mathrm{d}l \tag{6}$$

where l is the distance from the origin to current integral point along the line; $f(x, y)$ is the image function at point (x, y), and p is the projection function of $f(x, y)$. The image function $f(x, y)$ can be reconstructed uniquely through the definite projection function from the infinite Radon transformations. Recently, many solutions such as Abel transform, Fourier transform, MART technique and MLEM technique have been developed in different applications (Xu, 2003). In this study, maximum probability, a distinctive solution algorithm for tomographic inversion developed by Degenstein (1999), is applied to retrieving the two-dimensional atmospheric constituent profiles.

The VER of airglow can be estimated by the following iterative expression (Degenstein, 1999).

$$E_j^{(k)} = E_j^{(k-1)} \sum_i \left(\frac{B_i}{B_{i\mathrm{est}}^{(k-1)}} \beta_{ij} \right) \tag{7}$$

where $E_j^{(k)}$ is the VER of grid j in the kth iteration; the initial estimate of VER ($E_j^{(0)}$) is the weighted average of all observed radiance (B_i) along the LOS_i for grid j, shown as Equation (8); β_{ij} is the weighting factor of observed radiance along the LOS_i for grid j, calculated by Equation (9); $B_{i\mathrm{est}}^{(k-1)}$ represents the estimated radiance of grid j along the LOS_i in the $(k-1)$th iteration, which can be calculated by Equation (10).

$$E_j^{(0)} = \sum_i \left(\frac{B_i}{\sum_j L_{ij}} \beta_{ij} \right) \tag{8}$$

$$\beta_{ij} = \frac{L_{ij}}{\sum_i L_{ij}} \tag{9}$$

$$B_{i\mathrm{est}}^{(k-1)} = \sum_j L_{ij} E_j^{(k-1)} \tag{10}$$

2.3.2 *Tomography improvements*

From Equation (7), it is involved with a large sparse matrix for radiance simulation and a large dataset during iterative estimate of VER. In other words, storage requirements and computation speed are critical for the tomographic inversion. Consequently, three improvements are proposed in this paper for making the computation process more smooth.

Firstly, serial tables are created for storage of parameters, including VER profile, grid index, and intercept of LOS through each grid, observed and estimated radiance (Fig. 2). This effective tomographic inversion are able to process all the grids simultaneously and look up parameters conveniently, which not only saves the storage space but also improves the compution speed.

Taking the VER of 5th grid (E_5) in the red as an example to explain the initial estimate of VER (Fig. 2a). The indices of all the LOSs through the 5th grid can be looked up from Fig. 2b, including LOS_2, LOS_3 and LOS_5. Accordingly, the corresponding intercepts of the 5th grid intersected by three lines of sight are obtained and marked in the red (Fig. 2d). In addition, the observed and estimated radiance along the LOS_i can also be found in Fig. 2c, marked in the light blue. Once the intercepts of the 5th grid intersected by the LOS are known, it is possible to calculate the initial value of VER of the 5th grid by Equation (8). The estimated radiance ($B_{i\mathrm{est}}$) could be conducted by Equation (10), where the VER of the jth grid can be gotten from Fig. 2a and the intercept of the jth grid intersected by the LOS_i is the same as mentioned during the initial estimate of VER. Meanwhile, the initial VER in Fig. 2a will be updated by the next VER. Based on the initial VER, the VER can be calculated by the iterative Equation (7).

Secondly, the index and weighting factor of LOS through each grid in initial estimate is stored in order to be looked up directly in the later iterative calculation. This improvement could avoid computation repeatedly, and save the calculating time.

Thirdly, before inner summing of Equation (7), the product (B_i') of observed radiance along the LOS_i and the corresponding weighting factor, which is obtained in initial iteration process, is stored for the iteration later. Then the iterative Equation (7) can be rewritten as follows after this improvement.

$$E_j^{(k)} = E_j^{(k-1)} \sum_i \left(\frac{B_i'}{B_{i\mathrm{est}}^{(k-1)}} \right) \tag{11}$$

where $B_i' = B_i \cdot \beta_{ij}$, named as weighted observed radiance. With the improvements, the flowchart for VER inverison by tomographic technique is shown in Fig. 3.

E_{25}	E_{20}	E_{15}	E_{10}	E_5
E_{24}	E_{19}	E_{14}	E_9	E_4
E_{23}	E_{18}	E_{13}	E_8	E_3
E_{22}	E_{17}	E_{12}	E_7	E_2
E_{21}	E_{16}	E_{11}	E_6	E_1

(a) VER profile (E_j)

LOS_1	2	4	5	8	10	13
LOS_2	5	6	7	12	14	0
LOS_3	3	5	11	0	0	0
LOS_4	2	7	8	13	14	0
LOS_5	1	2	4	5	10	14

(b) Index of grid (j) intersected by LOS

LOS_1	B_1	
LOS_2	B_2	B_{2est}
LOS_3	B_3	B_{3est}
LOS_4	B_4	
LOS_5	B_5	B_{5est}

(c) Observed (B_i) and estimated radiance (B_{iest})

LOS_1	1.3	1.6	2.5	2.1	1.8	1.1
LOS_2	1.2	2.6	5.7	1.2	1.4	0
LOS_3	3.2	1.9	1.1	0	0	0
LOS_4	1.4	3.7	3.8	1.3	1.4	0
LOS_5	4.3	2.1	1.2	1.6	1.7	1.9

(d) Intercept (L_{ij}) of LOS_i intersected with grid j

Fig. 2 Serial tables for storage of parameters related to iterative process

3 Results

3.1 Radiance simulation results

It is noted previously that a two-dimensional VER profile is required for the radiance simulation. In this study, a 2D VER profile covering from 14.3° to 121.3° which corresponds to around 1/3 orbit (120°) is assumed to be as the input for simulating radiance (Fig. 4), which is a typical emission profile in the daytime based on the OIRA band with angular resolution of 0.2° and altitude resolution of 1 km.

Based on Equation (2), the radiance is simulated through the model of the limb observation mentioned above with the tangent altitude of optical axis of 40.5 km and imaging frequency of 0.5 Hz (Fig. 5). The simulated radiance is illustrated as a 700 images observation set and each image consists of 100 pixels. The maximum of radiance occurs at the 20th pixel in the around 200th and 550th images due to the similar structure of assumed VER profile. While the radiance decreases with the increasing pixel number, and almost equals to zero when the pixel is more than 60.

3.2 Volume emission rate inversion of airglow

Figure 6 is the final inversed VER profile through improved tomographic technique after 40 iterations. The structure of final estimate of the VER profile is almost the same as the assumed VER profile (Fig. 4), except for the obvious differences at the left and right edges of VER profile. This edge error may be due to the geometry of the observations which causes an under sampling of the grids in these regions, which must be discarded from each inversion.

The accuracy of tomographic inversion is performed by comparison of error between retrieved and assumed VER profiles for different iterations. Also, the error distribution of simulated radiance based on these VER profiles is also shown in Fig. 7. The number of grid whose corresponding error is less than ±20% is calculated in order to remove the poorly inversed data, especially the area with edge effect. Then the error distribution histograms with an interval of 10% between retrieved and assumed VER profiles after 10 and 40 iterations are formed, and corresponding quadratic fits are made (Fig. 7). The two parameters, full width at half maximum (FWHM) of error and the offset of the peak percentage from 0% of quadratic fit, are used to assess the inversion accuracy. From Fig. 7, the FWHM of the error is 8.34% and the offset of the peak percentage is –0.59% for final VER after 10 iterations, and the FWHM is 1.78% and

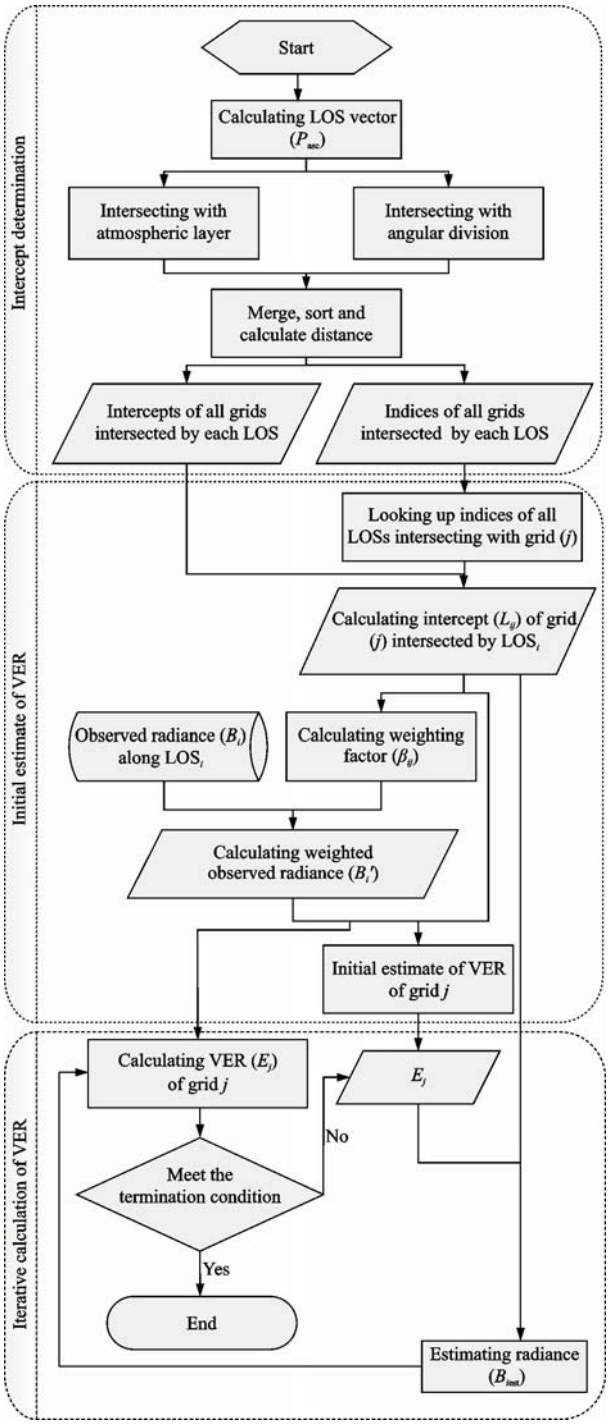

Fig. 3 Flowchart of improved tomographic technique for VER inversion

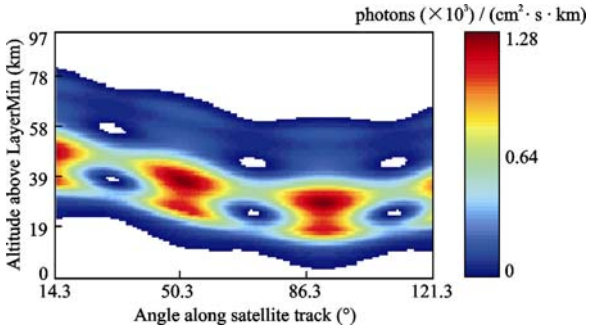

Fig. 4 Assumed VER profile for radiance simulation

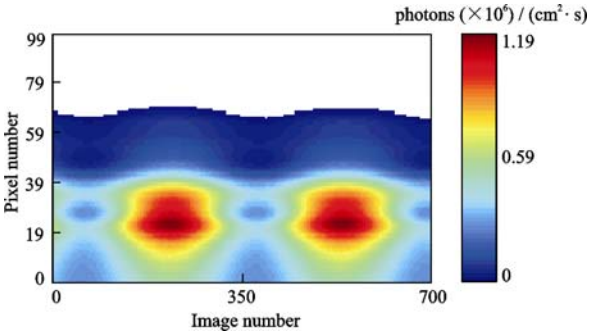

Fig. 5 Simulated radiance using assumed VER profile

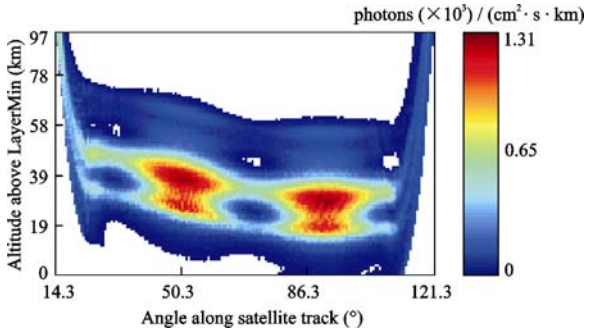

Fig. 6 Final VER profile through improved tomographic inversion after 40 iterations

the offset is 0.22% after 40 iterations. In addition, the FWHM and offset after 40 iterations are smaller than that after 10 iterations, so the accuracy of inversed VER after 40 iterations is higher. From Fig. 8, it can be found that there is no significant improvement after about 40 iterations. For this reason, the termination condition of VER inversion in this study is determined at 40 iterations.

The error of two vertical cross sections for retrieved and assumed VER profiles with angle 50.1° and 90.1° corresponding to the high VER region (Fig. 6) are shown in Fig. 9, which clearly illustrates the difference between the retrieved and assumed profiles at different altitudes above the Layermin. It shows that the error is almost limited within ±15% when the altitude is higher than 20 km and even less than ±8% when the atmospheric height is between 30 km and 60 km above the LayerMin with vertical resolution of 1 km.

For different images, the run time for iterative calcu-

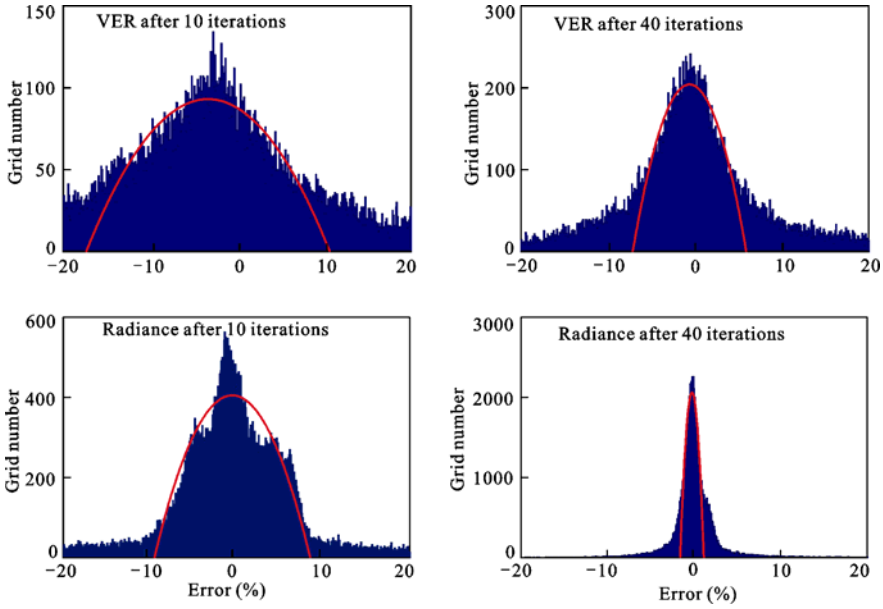

Fig. 7 Error distribution histogram of VER and radiance for 10 and 40 iterations

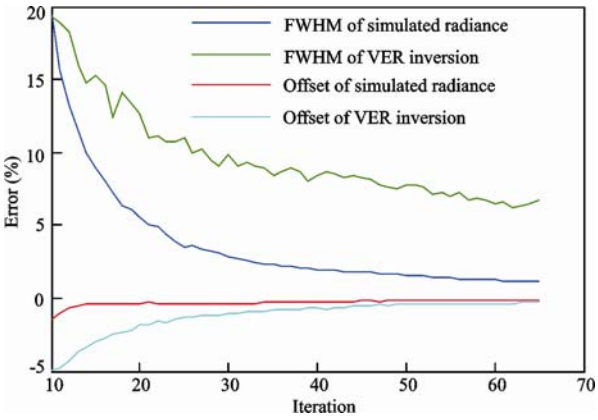

Fig. 8 FWHM and offset for retrieved VER and radiance

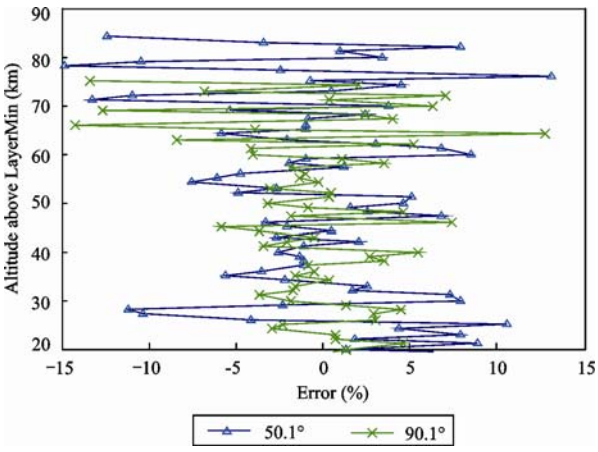

Fig. 9 Error of vertical cross sections of retrieved and assumed VER profiles

lation of tomographic inversion is showed in Fig. 10. By the comparison, the run time of VER inversion by using the tomographic technique before improvements is as much as 3 hours and 11 minutes, and it only costs 6 minutes with the improved tomography. The acceleration rate after improvements increases from 18.6% to 29.6% with images increasing from 100 to 700. Consequently, the improvements to tomographic inversion of VER are apparently effective and reliable.

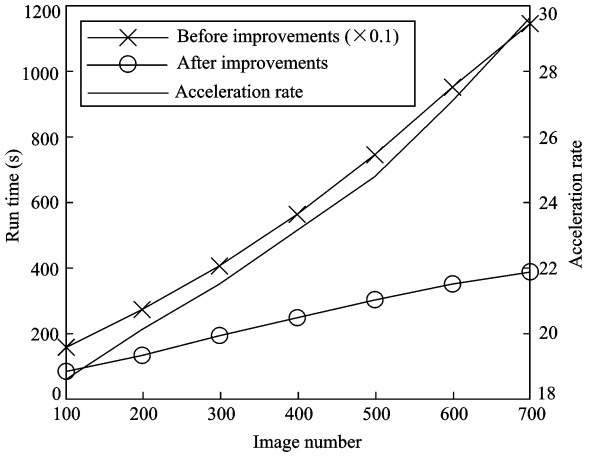

Fig. 10 Run time and acceleration rate with different images before and after improvements

4 Conclusions

Based on the assumed VER profile, the radiance meas-

urements are simulated by the model of satellite-based limb observation. The tomographic technique based on the maximum probability is applied to retrieving 2D VER profile from the simulated infrared radiance. In order to save the storage space and improve the computing speed, the improvements are made for tomographic inversion. By the iterative equation, the VER of airglow is retrieved by using the improved tomographic method.

(1) Based on the model of the limb observation, a radiance profile including 700 images is simulated. The maximum radiance occurs at the 20th pixel in the around 200th and 550th images due to the similar structure with the assumed VER profile. The radiance decreases with the increasing pixel count, and almost equals to zero when the pixel is more than 60.

(2) To meet the need of storage space and optimize the computing speed, three improvements for iterative calculation are proposed. Through comparison of computation time before and after the improvements, it illustrates that the computing speed can be improved by 29.6 times when retrieving 700 images with improved tomographic inversion, i.e. the processing time will be reduced from 3 hours and 11 minutes to only 6 minutes after the improvements for 1/3 orbit data.

(3) A VER profile is retrieved using the improved tomographic technique from the limb measurement. The structure of final retrieved VER profile is almost the same as that of assumed VER profile. The FWHM of the fit for the inversion on noiseless data is 1.78% and the offset of the peak error is 0.22% after 40 iterations for final VER. The error of the selected vertical cross sections at 50.1° and 90.1° for retrieved and assumed VER profiles fall within ±15% between 20 km and 90 km above the LayerMin, and even less than ±8% from 30 km to 60 km with vertical resolution of 1 km.

In conclusion, the improved solution algorithm for tomography is apparently effective for VER inversion of airglow from the satellite-based limb measurement. The application of tomography to remote sensing field is feasible and possesses important scientific significance.

References

Cormack A M, 1963. Representation of a function by its line integrals, with some radiological applications. *Journal of Applied Physics*, 34(9): 2722–2727. doi: 10.1063/1.1729798

Cormack A M, 1964. Representation of a function by its line integrals, with some radiological applications II. *Journal of Applied Physics*, 35(10): 2908–2913. doi: 10.1063/1.1713127

Degenstein D A, 1999. Atmospheric volume emission tomography from a satellite platform. Saskatoon: University of Saskatchewan

Degenstein D A, Bourassa A E, Roth C Z *et al*., 2008. Limb scatter ozone retrieval from 10 to 60 km using a Multiplicative Algebraic Reconstruction Technique. *Atmospheric Chemistry and Physics Discussion*, 8(3): 11853–11877. doi: 10.5194/acpd-8-11853-2008

Degenstein D A, Llewellyn E J, Lloyd N D, 2003. Volume emission rate tomography from a statellite platform. *Applied Optics*, 42(8): 1441–1450. doi: 10.1364/AO.42.001441

Dribinski V, Ossadtchi A, Mandelshtam V A *et al*., 2002. Reconstruction of Abel-transformable images: The Gaussian basis-set expansion Abel transform method. *Review of Scientific Instruments*, 73(7): 2634–2642. doi: 10.1063/1. 1482156

Evans W F J, Llewellyn E J, 1972. Observations of mesospheric ozone from observations of the 1.27 μ band. *Radio Science*, 7(1): 45–50. doi: 10.1029/RS007i001p00045

Fleming H E, 1982. Satellite remote sensing by the technique of computed tomography. *Journal of Applied Meteorology*, 21(10): 1538–1549.

Frey S, Mende S B, Frey H U, 2001. Satellite limb tomography applied to airglow of the 630 nm emission. *Journal of Geophysics Research*, 106: 21367–21380.

Gordonb R, Benderb R, Hermanb G T, 1970. Algebraic Reconstruction Techniques (ART) for three-dimensional electron microscopy and X-ray photography. *Journal of Theoretical Biology*, 29(3): 471–481. doi: 10.1016/0022-5193(70)90109-8

Khabibrakhmanov I K, Degenstein D A, Llewenllyn E J, 2002. Mesospheric ozone: Determination from orbit with the OSIRIS instrument on Odin. *Canadian Journal of Physics*, 80(4): 493–504. doi: 10.1139/p02-022

McDade I C, Llewellyn E J, 1993. Satellite airglow limb tomography: Methods for recovering structured emission rates in the mesospheric airglow layer. *Canadian Journal of Physics*, 71(11–12): 552–563. doi: 10.1139/p93-084

McDade I C, Lloyd N D, Llewellyn E J, 1991. A rocket tomography observation of N_2^+ 3914 Å emission in an Auroral Arc. *Planetary and Space Science*, 39(6): 895–906. doi: 10.1016/0032-0633(91)90094-Q

Noël S, Bovensmann H, Wuttke M W *et al*., 2002. Nadir, limb, and occultation observations with SCIAMACHY. *Advances in Space Research*, 29(11): 1819–1824. doi: 10.1016/S0273-1177(02)00102-3

Puro A, 2001. Cormack-type inversion of exponential Radon transform. *Inverse Problems*, 17(1): 179–188. doi: 10.1088/0266-5611/17/1/313

Roble R G, Hays P B, 1972. A technique for recovering the vertical number density profile of atmospheric gases from planetary occultation data. *Planetary and Space Science*, 20(10): 1727–1744. doi: 10.1016/0032-0633(72)90194-8

Rusch D W, Mount G H, Barth C A *et al*., 1984. Solar mesosphere explorer ultraviolet spectrometer: Observations of ozone in the

1.0–0.1 mbar region. *Journal of Geophysical Research*, 89(D7): 11677–11687. doi: 10.1029/JD089iD07p11677

Shepp L A, Vardi Y, 1982. Maximum likelihood reconstruction for emission tomography. *IEEE Transactions on Medical Imaging*, 1(2): 113–122. doi: 10.1109/TMI.1982.4307558

Solomon S C, Hays P B, Abreu V J, 1984. Tomographic inversion of satellite photometry. *Applied Optics*, 24(23): 3409–3414. doi: 10.1364/AO.23.003409

Solomon S C, Hays P B, Abreu V J, 1988. The auroral 6300 Å emission: Observations and modeling. *Journal of Geophysical Research*, 93(A9): 9867–9882. doi: 10.1029/JA093iA09p09867

Thomson F S, Tyler G L, 2007. Radon and Abel Transform equivalence in atmospheric radio occultation. *Radio Science*, 42(3): RS3024.1–RS3024.6. doi: 10.1029/2006RS003583

Wiensz J T, 2005. Ozone retrievals from the oxygen infrared channels of the OSIRIS infrared imager. Saskatoon: University of Saskatchewan

Xu Guoming, 2003. *Inverse Theory and Its Application*. Beijing: Seismic press. (in Chinese)